Pharm Res (2014) 31:2963–2974
DOI 10.1007/s11095-014-1391-6

RESEARCH PAPER

A Novel High-Speed Imaging Technique to Predict the Macroscopic Spray Characteristics of Solution Based Pressurised Metered Dose Inhalers

Nicolas A. Buchmann • Daniel J. Duke • Sayed A. Shakiba • Daniel M. Mitchell • Peter J. Stewart • Daniela Traini • Paul M. Young • David A. Lewis • Julio Soria • Damon Honnery

Received: 13 November 2013 / Accepted: 15 April 2014 / Published online: 17 June 2014

ABSTRACT

Purpose Non-volatile agents such as glycerol are being introduced into solution-based pMDI formulations in order to control mean precipitant droplet size. To assess their biopharmaceutical efficacy, both microscopic and macroscopic characteristics of the plume must be known, including the effects of external factors such as the flow generated by the patient's inhalation. We test the hypothesis that the macroscopic properties (e.g. spray geometry) of a pMDI spray can be predicted using a self-similarity model, avoiding the need for repeated testing.

Methods Glycerol-containing and glycerol-free pMDI formulations with matched mass median aerodynamic diameters are investigated. High-speed schlieren imaging is used to extract time-resolved velocity, penetration and spreading angle measurements of the pMDI spray plume. The experimental data are used to validate the analytical model.

Results The pMDI spray develops in a manner characteristic of a fully-developed steady turbulent jet, supporting the hypothesis. Equivalent glycerol-containing and non glycerol-containing formulations exhibit similar non-dimensional growth rates and follow a self-similar scaling behaviour over a range of physiologically relevant co-flow rates.

Conclusions Using the proposed model, the mean leading edge penetration, velocity and spreading rate of a pMDI spray may be estimated a priori for any co-flow conditions. The effects of different formulations are captured in two scaling constants. This allows formulators to predict the effects of variation between pMDIs without the need for repeated testing. Ultimately, this approach will allow pharmaceutical scientists to rapidly test a number of variables during pMDI development.

KEY WORDS co-flow · glycerol · HFA · high-speed schlieren imaging · modelling · pMDI

ABBREVIATIONS

ACI	Andersen Cascade Impactor
BDP	Beclomethasone dipropionate
FPD	Fine particle dose
HFA	Hydrofluoroalkane
MMAD	Mass median aerodynamic diameter
pMDI	Pressurised Metered Dose Inhaler

INTRODUCTION

The pressurised Metered Dose Inhaler (pMDI) is a well-established pulmonary drug delivery system (1,2). pMDI systems have an advantage over non-pressurised delivery systems since inhalation of the aerosol is aided by the expansion of the

N. A. Buchmann • D. J. Duke (✉) • S. A. Shakiba • D. M. Mitchell • J. Soria • D. Honnery
Department of Mechanical and Aerospace Engineering, Monash University, Melbourne, Victoria, Australia 3800
e-mail: daniel.duke@monash.edu

P. J. Stewart
Faculty of Pharmacy and Pharmaceutical Sciences, Monash University, Melbourne, VIC, Australia

D. Traini • P. M. Young
Respiratory Technology, Woolcock Insititute of Medical Research, University of Sydney, Sydney, NSW, Australia

D. Traini • P. M. Young
Discipline of Pharmacology, School of Medicine, The University of Sydney, Sydney, NSW, Australia

D. A. Lewis
Chiesi Limited, Chippenham, UK

N. A. Buchmann
Institute of Fluid Dynamics and Aerodynamics, Universität der Bundeswehr München, Neubiberg, Germany

J. Soria
Department of Aeronautical Engineering, King Abdulaziz University, Jeddah, Kingdom of Saudi Arabia

propellant. This imparts momentum on the aerosolised drug in addition to entrainment due to the patient's inhalation, leading to a more consistent effective dose (3). Modern particle sizing diagnostics also allow the aerosol particles to be engineered to target the alveoli and tracheo-bronchial regions as required (4).

The transition to hydrofluoroalkane (HFA) propellants has led to an increase in the use of co-solvents such as ethanol in order to produce effective pMDI solutions. This has led to a corresponding reduction in mean precipitant droplet size distribution, owing to the thermodynamic differences between formulations (5). As such, a range of non-volatile agents such as glycerol have been introduced into pMDI solutions to enlarge the mean precipitant droplet size (4,6,7). Lewis *et al.* (4) have developed solutions containing beclomethasone dipropionate (BDP) and a volatile mixture of HFA and an ethanol co-solvent, both with and without glycerol, with equivalent mass median aerodynamic diameter (MMAD). The ongoing goal is to study the biopharmaceutical outcomes in the lungs between formulations, so that the efficacy of glycerol-containing solutions can be evaluated independently of other variables (6). To match the effectiveness of glycerol-containing and glycerol-free formulations, both the microscopic and macroscopic properties must be characterised.

The microscopic properties of pMDIs have been extensively studied. Due to the high complexity and density of the flow close to the orifice (8), the resulting spray is usually studied far downstream from the nozzle where it is sufficiently dry and dilute, with stable particle size. Particle sizing can be achieved using systems such as the Andersen Cascade Impactor, Multi-Stage Liquid Impinger and Next Generation Impactor (9–11). Laser-based diagnostic methods are also prevalent (12,13). Laser velocimetry, diffraction and interferometry can also provide useful statistical measurements of particle velocity, shape and size (14).

In addition to matching the microscopic properties of the resultant spray, a number of macroscopic factors must also be considered. The atomization process (in which the spray forms as it exits the nozzle orifice) is controlled by not only the chemical formulation but also by transport phenomena (15). For example, entrainment with co-flowing inhaled air plays an important role in determining the macroscopic structure of the plume (16). Ross and Schultz (3) have investigated the effect of co-flow rate on the mean precipitant droplet size distribution, but the mechanisms occurring in the vicinity of the nozzle orifice are not well understood. Furthermore, the velocity at the leading edge of the plume is likely to be affected by compressible interaction with the surrounding gas which will cause a difference between the leading edge velocity and droplet velocities measured downstream (17).

Studies of the macroscopic properties of pMDIs in the near-field are critical in the design of pMDI systems in order to achieve high dose effectiveness and avoid excessive deposition of the drug in the oral cavity (18,19). Properties of interest typically include spreading angle and velocity of the spray plume. High-speed photographic and video imaging of pMDIs have been used to investigate these properties (8,20,21). High-speed imaging provides a wealth of information about the geometry of the plume, but extracting quantitative information is challenging due to the complexity of the flow.

Given the above considerations, it would be ideal to have a model to predict the plume geometry as a function of key design parameters such as orifice size and formulation properties without the need for repetitive laboratory testing. Rather than re-testing each new pMDI configuration to experimentally determine the macroscopic spray spreading angle and leading-edge velocity, applying an analytical approach, grounded in the underlying fluid mechanics of the spray, could inform the formulator of the optimum design conditions. In the automotive research field, significant effort has been invested in the development of techniques to analyse high-speed images of turbulent fuel sprays and to understand their global scaling properties (22,23). These techniques are equally applicable to pMDIs. For example, high-speed schlieren imaging (24) can be used to visualise the density field of the pMDI spray as well as its evolution in space and time.

In this paper, we develop a physics-based framework for predicting the behavior of a pMDI spray based on a small set of key non-dimensional scaling parameters. In order to confirm that this approach is indeed accurate, we apply the scaling to high-resolution measurements of spray tip displacement and velocity obtained using a high-speed schlieren imaging technique.

We show that two aerodynamically equivalent glycerol-containing and non glycerol-containing pMDIs follow self-similar scaling laws, once the appropriate non-dimensional time, length and velocity scales are implemented. This supports the hypothesis that the self-similar model captures the effects of varying formulation properties, orifice size and co-flow rates. The effect of orifice size and mixture properties are captured in two scaling constants which are empirically determined. The outcome of the study is a theoretical model which allows the spreading rates of pMDI sprays to be predicted within a controlled parameter space.

METHOD AND MATERIALS

An experiment is designed to make accurate measurements of the leading edge (front) of the spray plume as well as its cone angle (spreading rate). HFA-propelled pMDIs are repeatedly actuated in two different configurations. In the first configuration, the pMDI is actuated into quiescent air while in the second configuration an air co-flow is passed through the pMDI to simulate steady inhalation at various flow rates. In all cases the spray tip penetration, tip velocity, cone angle and

Table I Mass and Percentage Distribution for the Glycerol-Free and Glycerol-Containing pMDI Formulations

	Glycerol-free[a]		Glycerol-containing[b]	
	(mg)	(% b.w.)	(mg)	(% b.w.)
HFA 227	11.80	84.57	–	–
HFA 134a	–	–	14.58	84.30
Ethanol	2.09	15.00	2.60	15.00
BDP	0.06	0.43	0.06	0.35
Glycerol	–	–	0.06	0.35

[a] Metered dose: 50μL; Orifice: 0.33 mm

[b] Metered dose: 63μL; Orifice: 0.30 mm

their rates of change are measured as a function of time after start of actuation using non-intrusive schlieren imaging. The individual components of this experiment are explained in the following sections.

Solution-Based pMDI Formulations with Equivalent Aerodynamic Size Distribution

Two different pMDI formulations are designed to have an equivalent aerodynamic size distribution (4) and after evaporation of the volatile components contain either 250μg of drug (total non-volatile mass) or 250μg of drug and 250μg glycerol (=500μg of non-volatile mass). The first is a glycerol-free mixture containing pro-pellant HFA 127, ethanol and BDP in a ratio of 84.57, 15 and 0.43%. The second is a glycerol-containing formulation containing propellant HFA 134a, ethanol, BDP and glycerol in ratios of 83.4, 15, 0.35 and 0.35% respectively. The mass distribution of the volatile and non-volatile constituents of each mixture are listed in Table I. In order to ensure equivalent mass and stage deposition characteristics the glycerol-free formulation is ejected via a 50μL metering valve through a 0.33 mm diameter orifice, while the glycerol-containing formulation uses a 63μL metering valve and a 0.3 mm diameter orifice. The formulations are manufactured by adding BDP and the different concentrations of glycerol in the canister by weight. The canisters are then crimped with the respective valve and pressure filled with HFA using a Pamasol Laboratory plant 02016 (Pamasol Willi Maden AG, Paffikon, SZ) to a specific volume. Each pMDI contains 200 doses. The *in vitro* aerosol performance of the different formulations was assessed using an Andersen Cascade Impactor (ACI, Copley, UK) as detailed in Lewis *et al.* (4). The MMAD was 2.4±0.1 and 2.5±0.2μm and the fine particle dose (FPD, i.e. mass of particles <5μm) was 66±6 and 68±2μg for the glycerol-free and glycerol-containing solutions, respectively.

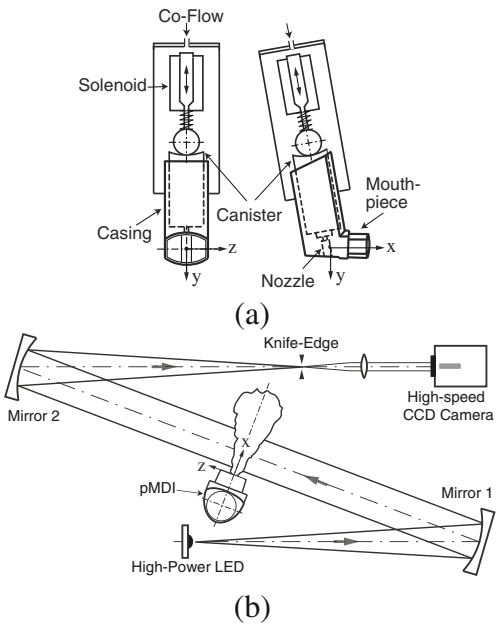

Fig. 1 (**a**) Schematic of pMDI setup and actuation; (**b**) Optical arrangement of the high-speed schlieren system and pMDI position.

Table II Flow Rate *Q*, Mean Velocity $\overline{U}$ and Peak Velocity $\widehat{U}$ of the Co-Flow at the Exit of the Mouth Piece

Co-flow	Q (lpm)	Q (slpm)	$\overline{U}_c$ (m/s)	$\widehat{U}_c$ (m/s)
A	0	0	–	–
B	20	21	1.27	2.53
C	40	54	3.13	5.04
D	60	90	5.35	10.15

Experimental Setup

The experimental arrangement consists of an automated actuated pMDI assembly and a Toepler Z-type schlieren

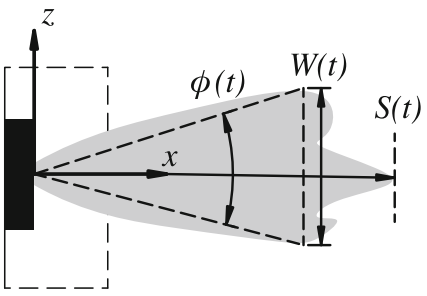

Fig. 2 Geometry of a typical pMDI plume, showing the co-ordinate system and the definition of penetration *S*(*t*), width *W*(*t*) and cone angle $\phi(t)$. The inhaler nozzle is indicated by the *black box*, and the mouthpiece is indicated by the *dashed box*.

apparatus (25) as shown in Fig. 1. The pMDI canister containing the different formulations is inserted into the casing, which contains the nozzle and mouthpiece. Prior to the experiment, the first five shots of each canister are fired to waste and the primed pMDI is mounted at a 15° angle to ensure that the plume exits the mouthpiece horizontally. The pMDIs are actuated repeatedly via a linear solenoid. Co-flow at prescribed flow rates through the pMDI is established by fitting a cylindrical casing around the pMDI and the actuator as shown in Fig. 1(a). The flow rates are controlled by an electronic mass flowmeter (Omega FMS-1610A) and set to 0, 20, 40 and 60 l per minute (see Table II). To avoid buildup and condensation in and around the mouthpiece, the casings are replaced and cleaned every 200 cycles (16).

Analysis is performed by means of schlieren imaging (25,24) to visualise density gradients in the mixed-phase flow, as shown in Fig. 1(b). In schlieren imaging, the density gradient is integrated along a line-of-sight, revealing dominant flow features above the mean density variation. Density gradients are observed in a single direction (i.e. $\partial\rho/\partial x$ or $\partial\rho/\partial r$) depending on the orientation of the focal point knife-edge. Although these will be discussed later, typical schlieren images of the inhaler flow are shown in Fig. 6.

Time-resolved image sequences of the transient flow are recorded with a high-speed camera (PCO Dimax) at 5 kHz with an exposure time of 1.3 μs. Illumination is provided by a high-power LED (Phlatlight PT-120 at $\lambda = 532$ nm), which is capable of producing μs light pulses at kHz repetition (26,27). The image magnification is 8.6 pixel/mm (magnification $\approx$ 11:1) and the resulting field of view is 232×232 mm^2 with the exit plane of the mouthpiece located at $x = 26$, $y = 0$ mm and the nozzle orifice at $x = 0$, $y = 0$ mm.

Measuring Spray tip Displacement and Velocity

The penetration (displacement) of the plume edge $S(t)$ at each time-step is defined by the point on the leading edge that has the maximum distance from the nozzle, as per Fig. 2. The velocity of the plume's tip is calculated as the rate of change of the tip penetration as $U(t) = dS/dt$. Measuring the tip penetration and tip velocity requires tracking of the leading edge. This is achieved using a Canny filter (28). The filter allows extraction of the tip penetration and velocity over time by isolating the boundary between the plume and the background.

To obtain a low uncertainty in the edge detection, it is important that the location of the detected edge is independent of the intensity threshold used to discriminated between the jet and the background in the recorded images (29). The factors which influence the uncertainty of an edge detection algorithm are multifaceted and more detail can be found elsewhere

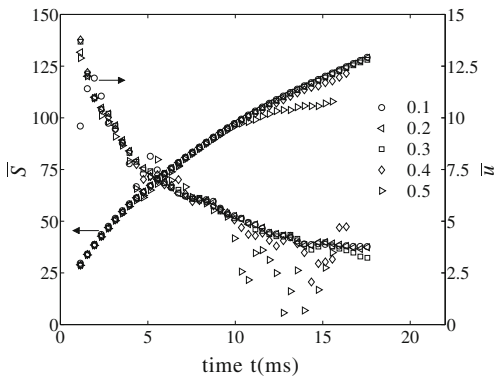

Fig. 3 Sensitivity in tip penetration and tip velocity for different threshold levels σ of the Canny edge detection routine. σ is expressed as a fraction of the image intensity range (0–1).

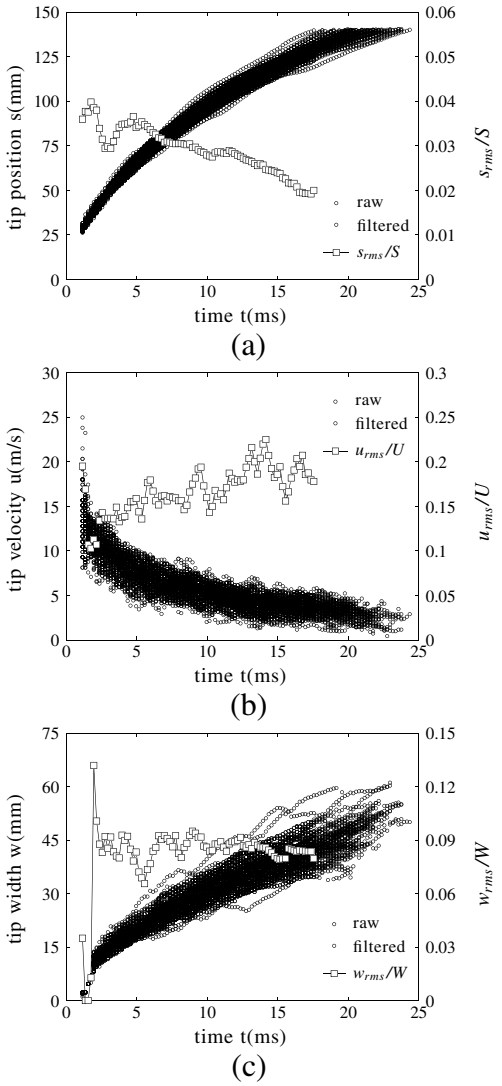

Fig. 4 Instantaneous (*gray circles*), fitlered (*black circles*) and normalised rms (*open squares*) flow properties: (**a**) tip position; (**b**) tip velcoity and (**c**) spray width.

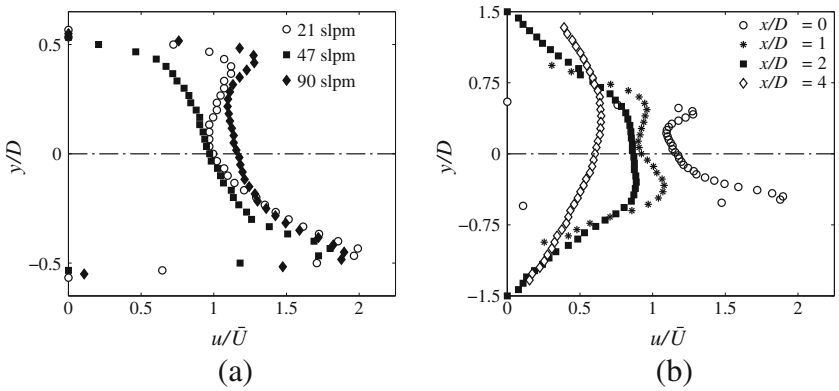

Fig. 5 Characterisation of the co-flow: (**a**) vertical profile of the axial velocity at the exit of the mouthpiece for 21, 47 and 90 slpm; (**b**) vertical profile of the axial velocity at locations $x/D = 0$, 1, 2 and 4 downstream of the mouthpiece, where D is the diameter of the mouthpiece.

(29–31). The sensitivity of the measured tip penetration and tip velocity to a range of intensity thresholds is shown in Fig. 3 for the glycerol-free pMDI at zero co-flow conditions. Close to the mouthpiece, limited mixing at the leading edge produces strong intensity gradients and the sensitivity in the intensity threshold is small in this area. As turbulent mixing becomes more dominant at the edge of the plume, sensitivity to the intensity threshold increases. To overcome this problem, a low threshold range of $\sigma \in [0.15, 0.2]$ was used in the measurements presented in this paper. Figure 3 shows that for threshold values in this range, the measurement is independent of the chosen threshold value and is unbiased.

In order to remove measurement outliers, the data are validated in a two step process. In the first step, each measurement point is compared with its neigh-bouring point by a local median test (32). The second validation step consists of a global histogram filter to exclude measurement points that vary by more than three standard deviations from the sample mean at a given time step. Applying these two validation steps improves the convergence of the statistical results, retaining 80–85% of the data points.

The effectiveness of the filtering is shown in Fig. 4. 70 events for the glycerol-free pMDI at zero co-flow are shown. This figure shows that significant shot-to-shot variations occur between pMDI events which must be accounted for. Assuming these variations are stochastic, uncertainties in the mean quantities ($\overline{S}$

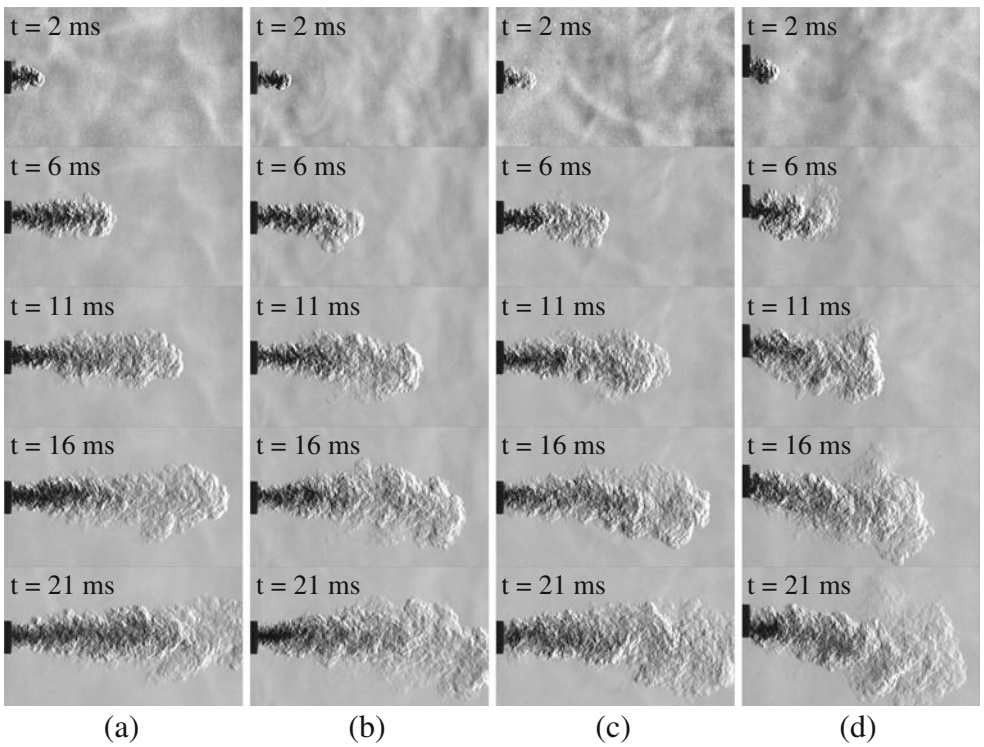

Fig. 6 Sequence of instantaneous schlieren images for the glycerol-free pMDI at co-flow rates of (**a**) 0 slpm; (**b**) 21 slpm; (**c**) 47 slpm and (**d**) 90 slpm. The knife edge filter is aligned to show $\partial \rho / \partial x$.

(t), $\overline{U}(t)$) at the 95% confidence level are ±0.5–1% for the tip position and ±2.5–5% for the tip velocity. In the results that follow, for each condition over 5000 valid measurements are obtained at over 85 time steps, each consisting of 65–70 samples, in order to maintain the confidence intervals given above.

Spray Width and Cone Angle Determination

The plume's cone angle is defined using the method described by Kostas *et al.* (23), where a triangle is defined with the apex at the source and the base of the triangle located at some fraction of the tip penetration location $S(t)$. The width of the base of the triangle is determined by a threshold condition to locate the edge of the plume. The cone angle ϕ is then the angle subtended by the two sides of the triangle which meet at the apex, as shown in Fig. 2; $0.8S(t)$ has been defined as the location of the base of the triangle from which ϕ and the spray width $W(t)$ are defined. The upper and lower bounds of the plume at position $0.8S(t)$ are independently measured so as to account for asymmetries when calculating ϕ.

RESULTS AND DISCUSSION

Co-Flow Characterisation

The velocity field produced by the co-flow in the absence of any spray is shown in Fig. 5. The shape of the inhaler body and canister results in a highly asymmetric shear flow with a

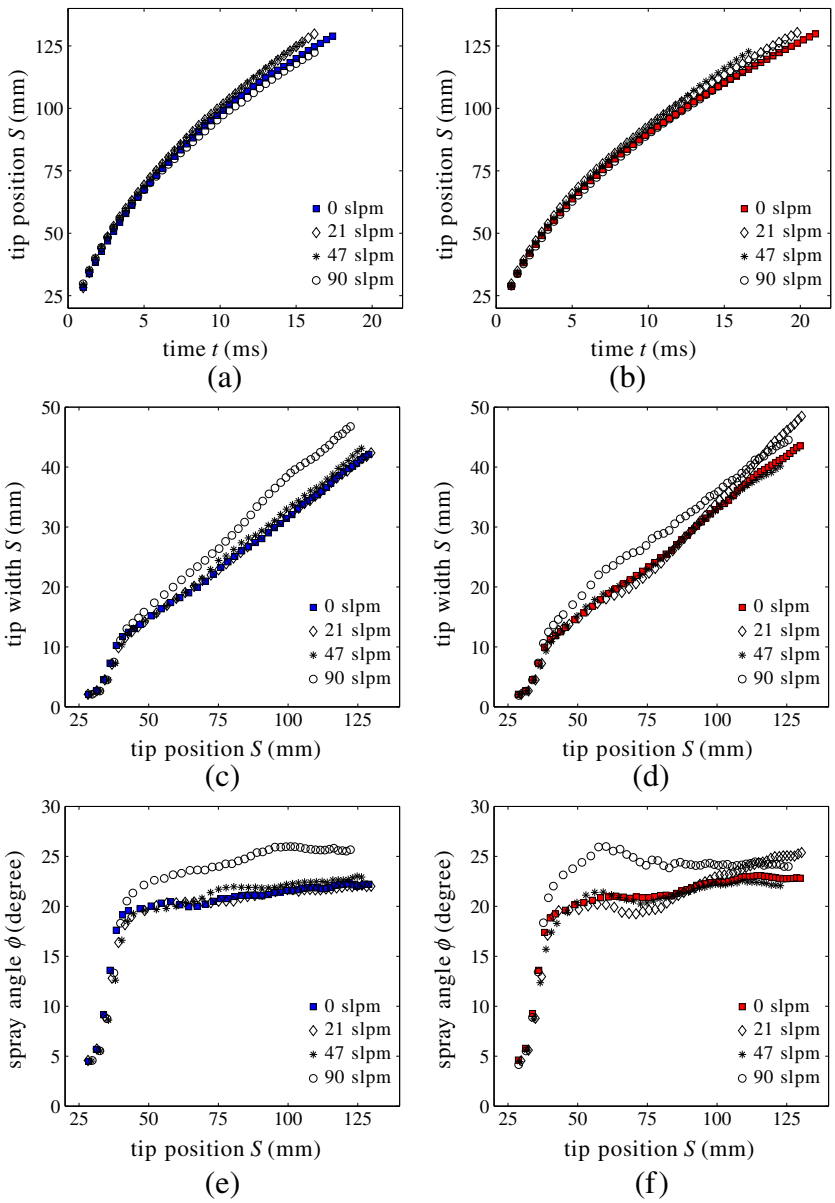

Fig. 7 (**a**,**b**)Mean axial tip penetration *versus* time; (**c**,**d**) mean width against tip penetration and (**e**,**f**) mean angle against tip penetration. Data are for different co-flow rates 0, 21, 47 & 90 slpm; (*left*) glycerol-containing pMDI (HFA 134a) and (*right*) glycerol-free pMDI (HFA 227). Time is taken relative to the start of the ejection (i.e. $t = 0$).

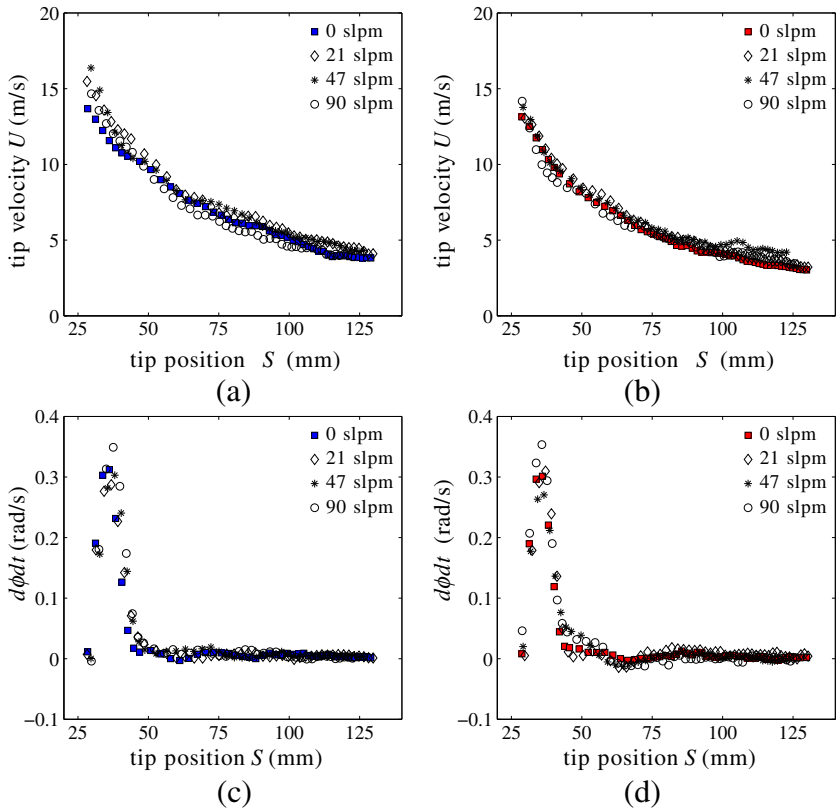

Fig. 8 (**a**,**b**) Mean axial tip velocity against tip penetration; (**c**,**d**) mean angle rate of change against tip penetration. Data are for different co-flow rates 0, 21, 47 & 90 slpm; (*left*) glycerol-containing pMDI (HFA 134a) and (*right*) glycerol-free pMDI (HFA 227). Time is taken relative to the start of the ejection (i.e. $t=0$).

non-uniform velocity profile due to the interior geometry of the pMDI. Since the canister and nozzle block the centre of the inhaler body, the velocity is lower in the centre and higher at the periphery. The angled shape of the inhaler body introduces an additional asymmetry of velocity profile, which will act to unevenly shear the aerosol spray in the vicinity of the mouthpiece. However, in the far-field these asymmetries have mostly disappeared at a distance of $x/D>1$ (Fig. 5(b)), where $D=15$ mm is the diameter of the mouthpiece.

Experimental Observations of Co-Flow and Propellant Formulation

The effect of the co-flow on the aerosol is shown in the raw schlieren images given in Fig. 6. At zero co-flow the spray plume appears axisymmetric, while at higher co-flow rates, the uneven shear causes the spray plume to deflect downwards (compare Fig. 6 bottom left to bottom right). Likewise the width of the spray appears to increase as the plume becomes asymmetric at higher co-flow rates.

A comparison of the tip penentation $S(t)$, tip width $W(t)$ and angle $\phi(t)$ for all experimental conditions is shown in Fig. 7. The time derivatives of these quantities (tip velocity $U(t)$, rate of change of width dW/dt and rate of change of angle $d\phi/dt$) are shown in Fig. 8 against the position of the tip from the nozzle in time. The velocities of the leading edge of the spray agree to order of magnitude with those of Clark (33), but with improved accuracy and resolution. Figures 7 and 8 show that

Table III Thermodynamic Properties and Reference Densities for the Different pMDI Propellants

Propellant	$\rho_{m,\gamma}$ (kg/m^3)	$\rho_{m,0}$ (kg/m^3)	p_{vap} (Pa $\times$ 10^5)	κ (cp/cv)	γ (liq. vol. frac.)
HFA 227	1167	121.61	4.56	1.039	0.84
HFA 134a	1019	123.62	6.65	1.052	0.85

Table IV Characteristic Length and Velocity Scales Used for Tip Penetration and Velocity Scaling

pMDI	Effective nozzle diameter d_e (mm)	Max. nozzle exit velocity[a] U_m (m/s)	Peak tip velocity[b] U_p (m/s)
glycerol-free (HFA 227)	3.4	17.70	15.33
glycerol-containing (HFA 134a)	3.0	24.05	21.06

[a] Eq. 7

[b] Eqs. 9 and 10, from (17)

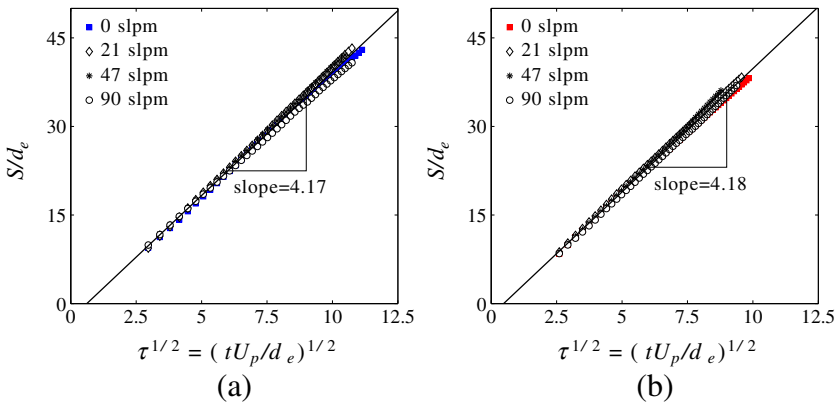

Fig. 9 Non-dimensional axial jet tip penetration S/d_e against non-dimensional time $\tau^{1/2} = (tU_p/d_e)^{1/2}$. Data are for different co-flow rates 0, 21, 47 & 90 slpm; (**a**) glycerol-containing pMDI (HFA 134a) and (**b**) glycerol-free pMDI (HFA 227).

the co-flow acts to change the width and angle of the spray due to mixing, but has little effect on penetration and velocity.

All inhaler flow measurements show a rapid non-linear increase in width and spreading angle in the early development region (Fig. 7(c–f)), and a corresponding peak in the width and angle time derivatives (Fig. 8(c–f)) at approximately 35–40 mm downstream of the nozzle. This initial rapid change in cone angle may be explained by the rapid expansion of the propellant, which initially accelerates plume widening. This expansion is counteracted by aerodynamic forces which act to reduce the spreading rate, until an equilibrium spreading rate is achieved and a nearly-constant cone angle of $\phi \approx 22–23°$.

The inhaler flow decelerates along the axial distance from the nozzle due to momentum exchange with the surrounding air, in agreement with previous observations (12,13). The deceleration and expansion of the flow is similar to that observed in other spray applications such as fuel sprays in internal combustion engines (34). In those applications, the expansion of the spray follows a fully-developed turbulent spray scaling in which the velocity decay follows a $U \propto 1/\sqrt{t}$ time response and therefore the penetration has a time response $S \propto \sqrt{t}$ (23). Figures 7 and 8 suggest that the pMDIs behave similarly.

Development of a Self-Similar Scaling Model

The above observations suggests the existence of a unified scaling law based on that for steady free jets. The high resolution measurements shown in Figs. 7 and 8 have a time response similar to a turbulent free jet, which have been shown to adhere to a self-similar one-dimensional scaling derived from a momentum balance of the flow's velocity distribution (22,23,17). This supports the hypothesis of a unified scaling law and if true, the data in Figs. 7(a–b) and 8(a–b) should collapse onto a line once the appropriate non-dimensional transformations are applied.

In the following, we determine the appropriate non-dimensional scales. Firstly, we express the penetration of the leading edge in terms of an effective nozzle diameter (35);

$$d_e = d_o \sqrt{\rho_{m,0}/\rho_a}, \tag{1}$$

where d_o is the nozzle diameter (Table I) and ρ_a is the ambient gas density. The argument behind Eq. 1 is that turbulent jets issuing into an environment of a different density undergo a change in diameter in order to accommodate the change in pressure (36). Since the pMDI jet is a flashing mixture, the

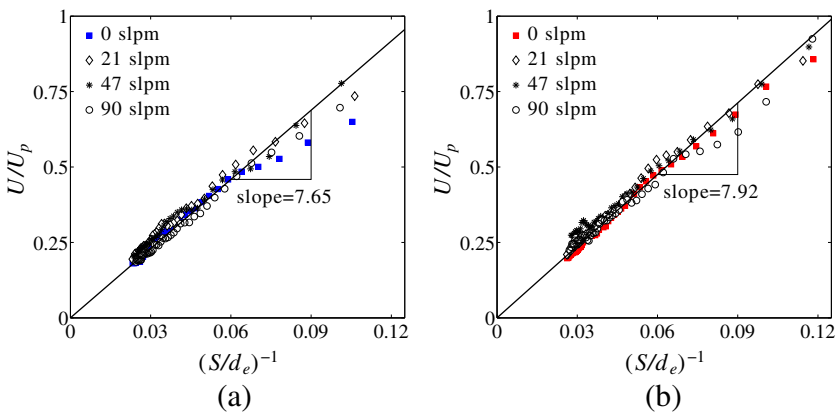

Fig. 10 Non-dimensional jet tip speed U/U_p against non-dimensional penetration $(S/d_e)^{-1}$. Data are for different co-flow rates 0, 21, 47 & 90 slpm; (**a**) glycerol-containing pMDI (HFA 134a) and (**b**) glycerol-free pMDI (HFA 227).

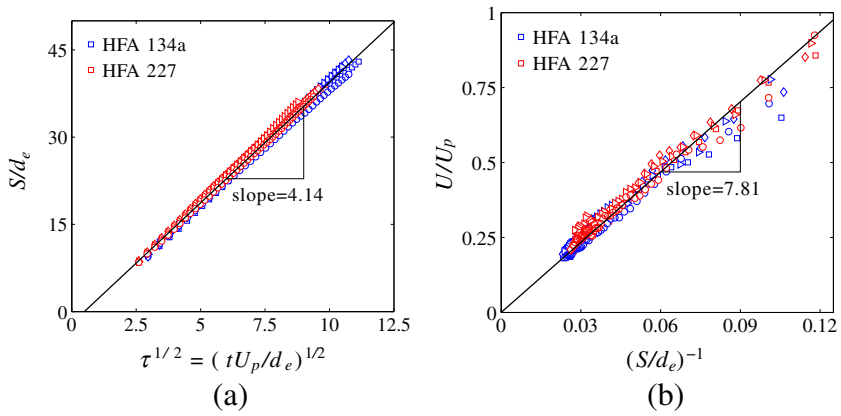

Fig. 11 (**a**) Non-dimensional axial jet tip penetration S/d_e and (**b**) non-dimensional jet tip speed U/U_p for the different propellants: (*blue*) HFA 134a, (*red*) HFA 227 for all co-flow rates.

density ($\rho_{m,0}$) of the mixture with propellant in the vapour state is used (37). This is supported by the schlieren images (Fig. 6), which appear to show evaporation of the ethanol occurring much further downstream. As such, the liquid ethanol (at 15% mass fraction) is the major determinant of $\rho_{m,0}$. The density ratio is approximately 100, making d_e an order of magnitude larger than d_o (see Table III).

Next we seek a velocity scale which explains the variations in velocity as a function of the drug formulation and spray conditions. Previous studies (23,17,13) suggest that compressibility effects at the leading edge are important and that the leading edge velocity scales with the peak velocity U_p of the spray tip, rather than the velocity of the spray at the orifice. Conversely, previous one-dimensional models such as those of Clark (33) do not include compressibility or the instantaneous non-equilibrium of the liquid and vapour phases. The peak velocity occurs very close to the nozzle exit, which is obscured in the present experiments by the mouthpiece. Therefore, the peak spray tip velocity is expressed using the model given in the Appendix that is of the following form

$$U_p = U_p(U_m, \kappa, \gamma, p_a, \rho_a) \tag{2}$$

where U_m, κ, γ, p_a and ρ_a are the respective jet exit velocity at the orifice, the propellant specific heat ratio, liquid volume fraction, ambient pressure and density and are tabulated in Tables III and IV for the pMDIs studied here.

A non-dimensional time scale (τ) is defined in terms of the aforementioned scales and the time t since start of ejection;

$$\tau = tU_p/d_e. \tag{3}$$

Since we know from previous studies that spray penetration $S \propto \tau^{1/2}$ (23,38), we introduce a scaling constant c such that

$$S(\tau)/d_e = c\,\tau^{1/2}. \tag{4}$$

Once the leading edge penetration S and velocity U are expressed in terms of the time scale τ and length scale d_e, self-similar development of the spray can be expressed through a non-dimensional spreading rate k (23), defined by the relation

$$\frac{U(\tau)}{U_p} = \left(\frac{k}{2}\right)^{1/2}\left(\frac{S(\tau)}{d_e}\right)^{-1}. \tag{5}$$

k is a scaling constant which defines the spreading rate of the jet. This model has been shown to provide a good representation in the far field of high-pressure fuel sprays (17,35). k can then be used to yield a value of the cone angle ϕ via the relationship

$$k = \frac{\ln(1/\zeta)}{\tan^2(\phi/2)}. \tag{6}$$

where ζ=0.01 demarcates the radial edge of the plume where the axial velocity has reduced to 1% of its centreline value (22,23).

Validating the Model with Experimental Data

The values of U_m, U_p, and d_e for the two pMDI solutions studied are given in Table IV. The values of U_p and U_m correspond well to the measured near-nozzle velocities in Fig. 8(a–b).

In Figs. 9 and 10, we apply the non-dimensional scaling by d_e, U_p and $\tau^{1/2}$ to the measurements of tip displacement and velocity. Figure 9 show that the measurements of S from Fig. 8(a–b) collapse linearly. This confirms that the axial

Table V Empirically Determined Scaling Constants c and k for Different pMDI Formulations and Co-Flow Rates. Values in parentheses Indicate the 95% Confidence Interval

Q (slpm)	Glycerol-free (HFA 227)		Glycerol-containing (HFA 134a)	
	c	k	c	k
0	4.07	117.4	4.14	107.8
21	4.21	131.9	4.33	127.7
54	4.42	136.5	4.32	128.0
90	4.18	118.0	3.96	106.6
	4.22 (0.20)	125.9 (13.5)	4.19 (0.24)	117.5 (16.6)

development of the spray in the far-field is proportional to $\tau^{1/2}$ (i.e. Eq. 4) and indicates that co-flow has little influence on this development. Assuming that the non-dimensional scaling for S is correct, we now look to validate Eq. 5. If true, we expect the gradient of U/U_p against $(S/d_e)^{-1} \equiv (k/2)^{1/2}$ to be constant. Figure 10 shows that this is true for most measurements confirming the self-similar development of the spray tip velocity (i.e. Eq. 5).

Next we consider the effect of the two propellant formulations and orifice geometries on the scaling constants. Figure 11(a) shows that the same linear trend is maintained between both formulations and for all co-flow rates. This indicates that the determined values of d_e, U_p and τ are universal across the two formulation and are independent of the co-flow rate.

Figure 11(b) shows that the slope defining k in Eq. 5 is also unaffected by the formulation, orifice geometries and co-flow rate. We find $(k/2)^{1/2} \approx 7.8$, yielding $k \approx 122$, and a mean cone angle of 21.9°. This is in very good agreement with the measured cone angle in the far field of approximately 22–23° in Fig. 7(e–f).

Table V summarises the determined scaling parameters c and k for the analytical pMDI spray model. Again, little variation is seen for the different pMDI designs and co-flow rates. The averaged value for the parameter describing the spray tip penetration is $c = 4.2 \pm 0.12$ and that for the spray angle is $k = 121.7 \pm 9.0$. Although only two formulations have been compared, the results suggest that the scaling hypothesis posed in Section 3.3 is sound. At the 95% confidence interval c varies by less than 3 and k by less than 8% across the two formulation and co-flow rates.

CONCLUSION

In this paper, we have proposed a non-dimensional self-similar scaling model for pMDI sprays. The advantage of this model is that the average spray spreading rate, leading edge displacement and velocity over time can be predicted with only two scaling constants derived from the orifice geometry and the thermophysical properties of the propellant. This allows the macroscopic characteristics of a pMDI spray to be estimated over a range of co-flow rates for a given formulation without the need for repeated laboratory testing.

The spray development model is based on non dimensional time and length scales based on a classical fully developed turbulent free jet. The non-dimensional velocity scale is based on the near-field peak velocity of a one-dimensional compressible jet model. The model has been validated using velocity and displacement measurements of the leading edge of the pMDI spray plume using high-speed schlieren imaging. Two aerodynamically equivalent pMDI formulations were considered, with and without glycerol. Experiments support the hypothesis that over a physiologically relevant range of co-flow rates, pMDI sprays behave like self-similar turbulent jets once an allowance for leading edge compressibility is made.

The model may be practically applied as follows. If testing for a particular formulation and known scaling constants k and c, the behaviour of a similar pMDI spray need not be re-tested, but can be estimated as follows.

- Knowing the properties of the formulation, co-flow environment and the orifice diameter, d_e, τ and U_p can be calculated as per Eqs. 1 and 7–10.
- Using $S(t)/d_e = c\,\tau^{1/2}$ allows the leading edge penetration $S(t)$ to be predicted (Eq. 4)
- Given $S(t)$, the leading edge velocity $U(t)$ can be calculated as per Eq 5.
- Finally, using Eq. 6 the spray spreading angle ϕ can be estimated from k.

In the case of unknown scaling constants, k and c can easily be determined by measuring the spray angle an penetration depth by imaging the spray at a fixed time after start of ejection.

High-speed imaging shows that the values of k for both the glycerol-containing and non glycerol-containing pMDIs yield predicted cone angles which match the experimentally derived spreading angle to within 2°. This indicates that past the point of peak velocity, flow development is effectively self-similar. Furthermore, both glycerol-containing and non glycerol-containing pMDIs show collapsed scaling behaviour and similar values for k and c. The aerodynamic shear to which the plume is exposed is nonuniform owing to the pMDI canister geometry, and causes a downwards redirection of the jet due to the increased vertical momentum of the co-flow. However, the non-dimensional collapse of penetration and velocity remain unaffected.

Estimates of the spray spreading angle, leading edge penetration and velocity may provide useful information to the formulator, without the need for extensive laboratory testing over multiple parameter spaces. For example, maintaining a certain range of k values ensures that the formulation does not have an overly wide or narrow spread angle. The time dependence of the velocity and leading edge penetration can provide useful information to the formulator about the required distance from the nozzle to the posterior pharyngeal wall for any physiologically relevant inhalation rate, and the efficacy of using a spacer device to avoid deposition.

ACKNOWLEDGMENTS AND DISCLOSURES

The authors would like to acknowledge the financial support of the Australian Research Council (grant number DP120103510).

APPENDIX

In order to calculate the peak velocity, we must first define the jet exit velocity at the orifice (39);

$$U_m = C_D\sqrt{2\left(p_{\text{vap}} - p_a\right)/\rho_{m,\gamma}}, \tag{7}$$

where p_{vap} is the propellant vapour pressure (as per Table III) and C_D is the nozzle discharge coefficient. $\rho_{m,\gamma}$ is the density of the propellant liquid-vapour mixture at the liquid fraction γ; it has been estimated using vapour and liquid state densities and quantities derived from thermodynamic tables for the respective propellants (40,41). C_D is solved using the known metered dosage of the drug and the average spray duration to estimate the mass flow rate m, which gives

$$C_D = \frac{\dot{m}}{A\sqrt{2\rho_{m,\gamma}\left(\rho_{\text{vap}} - \rho_a\right)}}, \tag{8}$$

where A is the nozzle area. For these experiments, we find $C_D \approx 0.8$, which is in very good agreement with the measurements of Clark (33) who found $C_D \approx 0.78$ for all conditions for a similarly designed metered dose aerosol. It should be noted that C_D can vary depending on the pMDI geometry, so care should be taken in assuming a value for C_D if the metering chamber and orifice dimensions are substantially altered (33).

Once U_m is known, the characteristic peak spray velocity U_p can be estimated using the model of Roisman *et al.* (17);

$$p_c(U_p) = p_a + \frac{1}{4}\left[(1+\kappa)\rho_a U_p^2 + \sqrt{\rho_a}U_0\sqrt{16\kappa p_a + (1+\kappa^2)\rho_a U_p}\right], \tag{9}$$

$$p_a + \left(\rho_{m,\gamma}.\gamma + \rho_a(1-\gamma)\right)\left(U_m - U_p\right)^2 = p_c(U_p), \tag{10}$$

where κ, γ, p_a and ρ_a are the propellant specific heat ratio, liquid volume fraction, ambient pressure and density respectively. Properties for the pMDIs studied here are given in Table III. p_c is the unknown pressure at the leading edge as a function of the peak tip velocity U_p; both variables are solved simultaneously in the above equations to yield $U_p = f(Um, \kappa, \gamma, p_a, \rho_a)$. We note that γ is an estimate, since the thermodynamic non-equilibrium of the mixture makes it difficult to know the state of the mixture at the nozzle. Models of pMDI sprays such as the one-dimensional models of Clark (33) cannot provide this information since they only indicate quantities at thermal equilibrium; the quantities at the nozzle exit during the transient spray are in a non-equilibrium state. Improving estimates for γ will be a matter for further investigation.

REFERENCES

1. Newhouse M. Advantages of pressurized canister metered dose inhalers. J Aerosol Med. 1991;4(3):139–50.
2. Finlay WH. The mechanics of inhaled pharmaceutical aerosols - an introduction. Academic Press; 2001.
3. Ross DL, Schultz RK. Effect of inhalation flow rate on the dosing characteristics of dry powder inhaler (DPI) and metered dose inhaler (MDI) products. J Aerosol Med. 1996;9(2):215–26.
4. Lewis DA, Young PM, Buttini F, Church T, Colombo P, Forbes B, *et al.* Towards the bioequivalence of pressurised metered dose inhalers 1: design and characterisation of aerodynamically equivalent beclomethasone dipropionate inhalers with and without glycerol 2 as a non-volatile excipient. Eur J Pharm Biopharm. 2013.
5. Keller M. Innovations and perspectives of metered dose inhalers in pulmonary drug delivery. Int J Pharm. 1999;186:81–90.
6. Haghi M, Bebawy M, Colombo P, Forbes B, Lewis DA, Salama R, *et al.* Towards the bioequivalence of pressurised metered dose inhalers 2. Aerodynamically equivalent particles (with and without glycerol) exhibit different biopharmaceutical profiles in vitro. Eur J Pharm Biopharm. 2013.
7. Brambilla G, Ganderton D, Garzia R, Lewis D, Meakin B, Ventura P. Modulation of aerosol clouds produced by pressurised inhalation aerosols. Int J Pharm. 1999;186(1):53–61.
8. Versteeg HK, Hargrave GK, Kirby M. Internal flow and near-orifice spray visualisations of a model pharmaceutical pressurised metered dose inhaler. J Phys Conf Ser. 2006;45(1):207.
9. Tzou TZ. Aerodynamic particle size of metered-dose inhalers determined by the quartz crystal microbalance and the Andersen cascade impactor. Int J Pharm. 1999;186:71–9.
10. May KR. Multistage liquid impinger. Bacteriol Rev. 1966;30:559–70.
11. Marple VA, Roberts DL, Romay FJ, Miller NC, Truman KG, Van Oort M, *et al.* Next generation pharmaceutical impactor (a new impactor for pharmaceutical inhaler testing). Part I: design. J Aerosol Med. 2003;16:283–99.
12. Liu X, Doub WH, Guo C. Evaluation of metered dose inhaler spray velocities using Phase Doppler Anemometry (PDA). Int J Pharm. 2012;423:235–9.
13. Dunbar CA, Hickey AJ. Selected parameters affecting characterization of nebulized aqueous solutions by inertial impaction and comparison with phase-Doppler analysis. Eur J Pharm Biopharm. 1999;48(2):171–7.
14. Ma Z, Merkus HG, de Smet JG, Heffels C, Scarlett B. New developments in particle characterization by laser diffraction: size and shape. Powder Technol. 2000;111(1):66–78.
15. Dunbar CA. Atomization mechanisms of the pressurized metered dose inhaler. Part Sci Technol. 1997;15(3–4):253–71.
16. Crosland BM, Johnson MR, Matida EA. Characterization of the spray velocities from a pressurized metered-dose inhaler. J Aerosol Med Pulm Drug Deliv. 2009;22(2):85–98.
17. Roisman IV, Araneo L, Tropea C. Effect of ambient pressure on penetration of a diesel spray. Int J Multiphase Flow. 2007;33:904–20.
18. Sweeney TD, Blanchard JD, Zeltner TB, Cater JE, Brain JD. Delivery of aerosolized drugs to the lungs with a metered-dose inhaler: quantitative analysis of regional deposition. J Aerosol Sci. 1990;21(3):350–4.
19. Clark AR. MDIs: physics of aerosol formation. J Aerosol Med. 1996;9(S1):19–26.
20. Smyth H, Hickey AJ, Brace G, Barbour T, Gallion J, Grove J. Spray pattern analysis for metered dose inhalers I: orifice size, particle size, and droplet motion correlations. Drug Dev Ind Pharm. 2006;32(9):1033–41.

21. Dhand R, Malik SK, Balakrishnan M, Verma SR. High speed photographic analysis of aerosols produced by metered dose inhalers. J Pharm Pharamcol. 1988;40:429–30.
22. Hajialimohammadi A, Honnery D, Abdullah A, Mirsalim MA. Time resolved characteristics of gaseous jet injected by a group-hole nozzle. Fuel. 2013;113:497–505.
23. Kostas J, Honnery D, Soria J. A correlation image velocimetry-based study of high-pressure fuel spray tip evolution. Exp Fluids. 2011;51: 667–78.
24. Settles GS. Schlieren and shadowgraph techniques. experimental fluid mechanics. Springer-Verlag; 2001.
25. Mitchell D, Honnery D, Soria J. The visualization of the acoustic feedback loop in impinging underexpanded supersonic jet flows using ultra-high frame rate Schlieren. J Vis. 2012;15(7):333–41.
26. Buchmann NA, Willert CE, Soria J. Pulsed, high-power LED illumination for tomographic particle image velocimetry. Exp Fluids. 2012;53:1545–60.
27. Willert CE, Mitchell DM, Soria J. An assessment of high-power light-emitting diodes for high frame rate schlieren imaging. Exp Fluids. 2012;53(2):413–21.
28. Canny J. A computational approach to edge detection. IEEE Trans Pattern Anal Mach Intell. 1986;8(6):679–98.
29. Duke D, Honnery D, Soria J. A comparison of subpixel edge detection and correlation algorithms for the measurement of sprays. Int J Spray Combust Dyn. 2011;3(2):93–109.
30. Duke D, Honnery D, Soria J. A cross-correlation velocimetry technique for breakup of an annular liquid sheet. Exp Fluids. 2010;49: 435–45.
31. Duke D, Honnery D, Soria J. Experimental investigation of nonlinear instabilities in annular liquid sheets. J Fluid Mech. 2011;691:594–604.
32. Westerweel J, Scarano F. Universal outlier detection for PIV data. Exp Fluids. 2005;39(6):1096–100.
33. Clark AR. Metered atomisation for respiratory drug delivery. Loughborough University; 1991.
34. Hiroyasu H, Arai M. Structures of fuel sprays in diesel engines. SAE J. 1990 Feb;900475.
35. Pastor JV, López JJ, García J, Pastor JM. A 1D model for the description of mixing-controlled inert diesel sprays. Fuel. 2008;87(13–14):2871–85.
36. Ricou FP, Spalding DB. Measurements of entrainment by axisymmetrical turbulent jets. J Fluid Mech. 1961;11(1):21–32.
37. Shaik AQ. Numerical modeling of two-phase flashing propellant flow inside the twin-orifice system of pressurized metered dose inhalers (PMDIs). Loughborough University; 2010.
38. Kostas J, Honnery D, Soria J. Time resolved measurements of the initial stages of fuel spray penetration. Fuel. 2009;88(11): 2225–37.
39. White FM. Fluid mechanics. 4th ed. Singapore: McGraw-Hill; 1999.
40. Ihmels EC, Horstmann S, Fischer K, Scalabrin G, Gmehling J. Compressed liquid and supercritical densities of 1, 1, 1, 2, 3, 3, 3-heptafluoropropane (R227ea). Int J Thermophys. 2002;23(6): 1571–85.
41. Huber ML, McLinden MO. Thermodynamic properties of R134a (1, 1, 1, 2-tetrafluoroethane). In: International Refridgeration and Air Conditioning Conference; 1992.